Ultra-high pressure disordered eight-coordinated phase of Mg$_2$GeO$_4$: Analogue for super-Earth mantles

R. Dutta[1,2*], S. J. Tracy[1], R. E. Cohen[1], F. Miozzi[1], K. Luo[1], J. Yang[1], P. C. Burnley[3], D. Smith[4], Y. Meng[4], S. Chariton[5], V. B. Prakapenka[5], and T. S. Duffy[2]

[1]Earth and Planets Laboratory, Carnegie Institution for Science, Washington DC 20015 USA.
[2]Department of Geosciences, Princeton University, Princeton, NJ 08544 USA.
[3]Department of Geoscience, University of Nevada, Las Vegas, NV 89154 USA.
[4]HPCAT, Advanced Photon Source, Argonne National Laboratory, Argonne, IL 60439 USA
[5]Center for Advanced Radiation Sources, University of Chicago, Chicago, IL 60637 USA.

Abstract

Mg$_2$GeO$_4$ is an analogue for the ultra-high pressure behavior of Mg$_2$SiO$_4$, so we have investigated magnesium germanate to 275 GPa and over 2000 K using a laser-heated diamond anvil cell combined with *in situ* synchrotron X-ray diffraction and density functional theory (DFT) computations. The experimental results are consistent with a novel phase with disordered Mg and Ge, in which germanium adopts eight-fold coordination with oxygen: the cubic Th$_3$P$_4$-type structure. Simulations using the special quasirandom structure (SQS) method suggest partial order in the tetragonal $I\bar{4}2d$ structure, indistinguishable from $I\bar{4}3d$ Th$_3$P$_4$ in our experiments. These structures have not been reported before in any oxide. If applicable to silicates, the formation of this highly coordinated and intrinsically disordered phase would have important implications for the interior mineralogy of large, rocky extrasolar planets.

Introduction

A large number of exoplanets have been discovered in recent years, including many planets whose mean density indicates they have rocky interiors that may be up to ten times more massive than the Earth (1). There is significant interest in understanding the mineralogy of the deep interiors of such bodies, where the pressure at the core-mantle boundary is predicted to reach up to 1 TPa (2–4). Theoretical calculations suggest that silicate structures with partial or

*Corresponding author: rdutta@carnegiescience.edu

complete eight-fold coordination of silicon can be stabilized above 500 GPa (4). These pressures are expected to be reached within the mantles of rocky exoplanets of ~ 4 Earth masses or greater (3, 4). Phase changes with accompanying changes in cation coordination number may strongly affect the structure, dynamics, and heat flow in exoplanet interiors (1, 5).

Germanates are known to be effective analogues for silicates as they undergo similar phase transitions, but at lower pressures (6, 7). For example, the perovskite (Pv) to post-perovskite (pPv) transition occurs near 65 GPa in $MgGeO_3$ (8) as compared to ~125 GPa in the corresponding silicate. Recently, a theoretical study has examined ultra-high pressure transitions in the $MgO-GeO_2$ system and suggest that it can be an excellent analogue system for ultra-high pressure phase transitions in silicate minerals (9). These calculations predicted that $MgGeO_3$ post-perovskite and MgO will combine to form an eight-coordinated tetragonal phase of Mg_2GeO_4 ($I\bar{4}2d$) at ~175 GPa (9) (Suppl. Material, Fig. S1). This transition pressure is experimentally accessible with a laser-heated diamond anvil cell. The same transition is predicted to occur at ~490 GPa (4) in the silicate, which is beyond the limit of conventional static compression techniques.

Here we report laser-heated diamond anvil cell experiments to examine Mg_2GeO_4 above 200 GPa, demonstrating that a cubic Th_3P_4-type ($I\bar{4}3d$) or partially ordered $I\bar{4}2d$ phase is synthesized under such conditions. Our computations suggest an unusual isostructural transition from an almost ordered tetragonal (order parameter Q = 0.81) to almost disordered tetragonal phase (Q = 0.25) at high temperatures. Disordered ions of very different valences, Ge^{4+} and Mg^{2+} is highly unusual, and perhaps occurs in other high-pressure systems at high temperatures. The calculations also reveal the atomic structure and pressure-volume relationship of the disordered phase. The formation of the Th_3P_4-type *or $I\bar{4}2d$* phase in the corresponding silicate at higher

2

pressures would have important implications for the interior mineralogy of large, rocky extrasolar planets.

Results

In a series of experiments (Suppl. Material, Table S1), Mg_2GeO_4 olivine samples were compressed to pressures between 115 and 275 GPa. Prior to any heating, the X-ray diffraction (XRD) patterns contained only gold and rhenium peaks, indicating the germanate underwent pressure-induced amorphization at these conditions (10). Figure 1 shows 300-K diffraction patterns obtained on Mg_2GeO_4 samples that had been heated above 2000 K at pressures between 161 and 275 GPa. A consistent set of new diffraction peaks is observed in all of these patterns. The ordered tetragonal $I\bar{4}2d$ structure was predicted by DFT to be more stable than $MgGeO_3$ pPv + MgO in this pressure range (9).We carried out theoretical calculations to optimize this structure at pressures relevant to our experimental conditions. A comparison of the new peaks observed in our experiments to those of the theoretically predicted $I\bar{4}2d$-type Mg_2GeO_4 phase show similarities in peak positions, but the expected splittings associated with the tetragonal phase are not observed (Suppl. Material, Fig. S2). This is suggestive of formation instead of a related higher symmetry phase. Under the assumption that the unit cell of the new phase is cubic; only a single indexing is possible, consistent with a body-centered-cubic lattice ($h + k + l = 2n$). Within the minimal supergroups of $I\bar{4}2d$ (#122), space group $I\bar{4}3d$ (#220) provides the only possible solution. Of ~40 candidate structure types for the AB_2X_4 stoichiometry (11), only one structure with this space group is known: the thorium phosphide structure, Th_3P_4 ($I\bar{4}3d$, Z=4). Fitting the observed diffraction data to this structure yields a good match to the peak positions (Suppl. Material, Table. S2).

The Th$_3$P$_4$-type Mg$_2$GeO$_4$ structure can be understood as an order-disorder transition of the tetragonal $I\bar{4}2d$ phase. The ordered tetragonal structure has two cation sites: Mg (*8d*) and Ge (*4a*), while O occupies the *16e* site. The Th$_3$P$_4$ structure is intrinsically disordered with both cations having partial occupancy of the *12a* Wyckoff site (Mg: 2/3, Ge: 1/3) while O occupies the *16b* site. At high temperature, a disordered phase can be stabilized relative to a corresponding ordered form by configurational entropy. While a phase exhibiting cation disorder between Mg^{2+} and Ge^{4+} might be considered a surprising result given the large difference in cation radius and valence, the energetics associated with different site occupancies across species may diminish under extreme compression. Firstly, we considered the relative stability of the ordered $I\bar{4}2d$ phase compared with the completely disordered cubic $I\bar{4}3d$. The disordering enthalpy increases significantly with pressure (70 – 342 GPa): $\Delta H/fu = 0.027\text{-}0.081$ Ryd (0.37-1.10 eV). Counteracting the enthalpy of disorder is the configurational entropy, which is zero in the completely ordered tetragonal $I\bar{4}2d$ and $S/k_B/fu = 1.90954$ for the cubic disordered phase. The transition from completely ordered tetragonal to completely disordered cubic is when the Gibbs free energy difference $\Delta G = 0$, thus ranges from 2233K-6718 K for 70-342 GPa (Fig. S3).

Although many minerals and alloys have sharp first-order or fairly sharp continuous transitions from nearly ordered to disordered structures, it is also possible to have other behaviors (12). The tetragonal structure can be partly disordered, with an order parameter, Q that varies from 0 for the disordered $I\bar{4}3d$ structure to 1 for the completely ordered $I\bar{4}2d$ phase. The relationship is $X_{Mg}(8d) = Q \times 1/3 + 2/3$ and $X_{Mg}(4a) = -Q \times 2/3 + 2/3$. This is known as convergent ordering, because the sites become equivalent when completely disordered. On varying the order parameter from $Q = 0$ to $Q = 1$ (Suppl. Material. Section. S4), we find a phase transition. The phase transition is not the transition from a completely ordered to completely

disordered structure, rather an isostructural first order phase transition within the tetragonal $I\bar{4}2d$ space group, from more ordered ($Q = 0.81$) to less ordered ($Q = 0.25$). The ΔS ordering is fairly flat (Fig. S6) from $Q = 0.2$ to $Q = 0$, whereas ΔH continues to increase, so it does not pay to completely order, even at huge temperatures (>10,000K). This comes from the large linear term in $\Delta H(Q)$ (12).

Figure 2a summarizes the transition curves for the order-disorder phase transition from this study and previous work (13). Our calculations yield transition temperatures higher than Ref. (13); insufficient information is given in that paper to determine the source of the differences, but possibly it is due to their smaller cell sizes. Increasing disorder leads to a decrease in the *c/a* ratio (Fig. 2b). The observed X-ray diffraction pattern is consistent with both the $Q = 0.25$ and 0.0 structures (Fig. 2c) and it is impossible to distinguish between the two, while the splittings expected for Q = 1 and 0.8125 are never observed. We estimate Q < ~0.53 cannot be distinguished experimentally. The diffraction patterns throughout the manuscript have therefore been indexed with the $Q = 0$ cubic $I\bar{4}3d$ Th_3P_4 structure (Fig 3, right) and has been referred to as the Th_3P_4-type phase for the experimental data. Further details of the Th_3P_4-type structure are provided in the supplementary material (Suppl. Material, Section. S3).

A heating cycle conducted at 234 GPa (H3_2) shows peaks from the Th_3P_4-type Mg_2GeO_4 phase grow with heating duration (~17 minutes heating time) and temperature (Suppl. Material, Fig. S8). We generated a disordered special quasirandom structure (SQS) using the ATAT toolkit (14) in a 224 atom supercell and optimized the structure using Quantum Espresso (15). The average structure was obtained using FINDSYM (16). The resulting structural parameters were used as an initial model to carry out a Rietveld refinement (Figure 3, left) of the

diffraction pattern quenched from peak temperature (3650 K). The corresponding two-dimensional image (Suppl. Material, Fig. S9) shows smooth diffraction rings.

The lattice parameters and atomic positions obtained from the experiments and computations are in good agreement with each other (Table. S3). The unit cell dimension from the Rietveld refinement of the experimental data at 184 GPa is 5.4930 Å, while the calculations yield 5.492 Å at 193 GPa. The Mg-O and Ge-O bond lengths from the experiments (theory) are 2.080 Å (2.015 Å) and 1.745 (1.796 Å). If the O is placed at the ideal x value for the Th_3P_4 structure ($x = 1/12$), the Mg-O and Ge-O bond lengths would be 1.903 Å and 1.898 Å. Whereas the difference in the Mg-O and Ge-O bond lengths suggest a substantial distortion of the cation site, it is consistent with an increase in coordination (~5% increase in bond lengths) from the post-perovskite $MgGeO_3$ (Mg-O: 1.94 Å and Ge-O: 1.70 Å) structure (17) at 184 GPa.

The pressure-temperature conditions achieved in our experiments are shown in Figure 4. For our lowest pressure experiment (115 GPa), the diffraction peaks obtained during heating (Fig. S10) can be assigned to $MgGeO_3$ post-perovskite ($Cmcm$) and B1-MgO ($Fm\overline{3}m$), and no evidence for formation of an Mg_2GeO_4 phase was observed. These results are consistent with theoretical predictions at this pressure (Fig. S1). It is also notable that prolonged heating near 2000 K was required at this pressure to produce any diffraction peaks at all, suggesting that the decomposition of Mg_2GeO_4 into post-perovskite and periclase (MgO) may be kinetically slow due to the atomic diffusion required for the decomposition reaction.

For experiments between 130 and 170 GPa, the results are more complicated. The diffraction data are consistent with the Th_3P_4-type (or $I\overline{4}2d$, $Q = 0.25$) phase upon initial heating of the amorphous sample. However, upon prolonged heating and/or at higher temperatures, peaks of the post perovskite phase emerge (Fig. S11 and Table S5) and grow at the expense of

Th$_3$P$_4$-type peaks e.g. Figure 4 (top right). In the higher-pressure runs above 175 GPa, peaks consistent with the Th$_3$P$_4$-type phase are observed to form and/or grow during heating in all experiments. For example, in one run (H2_2), the pPv phase was synthesized at lower pressures and then the pressure in the cell was increased to 175 GPa. Upon heating at this pressure, the post-perovskite peaks diminish over time while Th$_3$P$_4$-type peaks grow (Fig. 4 bottom right). Complete transformations from Mg$_2$GeO$_4$ to MgGeO$_3$ + MgO and vice versa are not observed because of the slow reaction kinetics. In run H4, a fresh sample was heated at 187 GPa, and only Th$_3$P$_4$-type peaks were observed within ~ 2 minutes of laser heating and retained even after prolonged heating to 3000 K.

These observations point to the conclusion that below 175 GPa, the new Mg$_2$GeO$_4$ phase is a metastable phase formed on initial heating in this pressure range. The metastable behavior can be understood as a result of transformation kinetics of the highly coordinated amorphous phase that forms on room-temperature compression. Experiments on germania glass show that the Ge-O coordination number increases with compression reaching a value greater than 7 at 92 GPa (18), and it likely continues to grow with pressure. Therefore, on initial heating at lower temperatures, it may be kinetically easier to transform to the cation-disordered, eight-fold coordinated phase of Mg$_2$GeO$_4$, rather than decompose into the six-fold coordinated, cation-ordered post-perovskite phase and MgO. Similar behavior has been observed in experiments on the SiO$_2$ polymorph cristobalite, in which seifertite, a phase that is thermodynamically stable at pressures above 100 GPa, was observed to form metastably on heating at pressures as low as ~11 GPa, within the stability field of stishovite (19). This was interpreted as a result of the faster kinetics for the formation of metastable seifertite from the cristobalite X-I phase. Upon

prolonged heating to higher temperatures, seifertite eventually transformed into the

thermodynamically stable stishovite structure, similar to the behavior we observe here.

The question remains as to why the theoretically predicted ordered $I\bar{4}2d$ phase is never

observed in our experiments. The minimum temperature that could be measured on heating was

~1200 K, which combined with the expected slow transformation kinetics at such temperatures

prevents us from obtaining any constraints on phase stability at low temperatures. The fast

quench rate in laser-heated diamond anvil cell experiments likely precludes a transition to the

tetragonal ordered phase upon cooling. Substitutional ordering requires site diffusion that may be

kinetically limited at multi-Mbar pressures. In run H4, we attempted to decrease the laser power

in small steps to replicate slow cooling (3032 K to 300 K in ~14 minutes). The ordered $I\bar{4}2d$

phase was still not observed. We should also consider the instrumental, thermal, and possible site

disorder broadening, which may make it difficult to distinguish the tetragonal phase splittings.

Further work will be necessary to better determine if the $I\bar{4}2d$ phase can be synthesized at lower

temperatures.

Figure 5a shows the pressure-volume relation of the Th_3P_4-type Mg_2GeO_4 phase at 300 K

(0 K theoretically). No pressure-transmitting medium was used in these experiments to maximize

the sample volume at extreme pressures. To minimize the effect of differential stresses on the

experimental results, we have included only data points obtained immediately after quenching

from high-temperature at each pressure step. Theoretical calculations were also performed to test

the reliability of the equation of state parameters. A third-order Birch-Murnaghan fit (solid:

experiments; dashed: theory) to the data yields $V_0 = 252.5$ (3.2) Å^3, $K_{0T} = 188$ (11) GPa and $V_0 =$

261.6 (1.2) Å^3, $K_{0T} = 170$ (3) GPa respectively; K'_{0T} was fixed at 4 in both cases. The ambient-

pressure bulk modulus is comparable to that of the pPv (8) $MgGeO_3$ phase (K_{0T} = 192 (5) GPa, K'_{0T} = 4).

Figure 5b compares the densities of phases in the MgO-GeO_2 system (17, 20–25). The densities of $MgGeO_3$ + MgO mixtures were calculated assuming an ideal solid solution (i.e., the molar volumes are additive). The density of the mixture (ρ) is given by:

$$\frac{1}{\rho(P,T)} = \frac{(1-m_2)}{\rho_1(P,T)} + \frac{m_2}{\rho_2(P,T)},$$

where m and ρ are the mass fraction and density of the individual components. Our results indicate that the transition from post-perovskite and MgO to the Th_3P_4-type phase produces a substantial (2.4%) change in density ($\Delta\rho$) at 190 GPa.

Discussion

Changes in silicon coordination in minerals can influence the structure and dynamics of planetary interiors. The transition in silicates from tetrahedral (four-fold) to octahedral (six-fold) coordination of silicon by oxygen occurring near 660-km depth defines the major structural boundary in Earth's mantle (26). In the Earth, six-coordinated silicate phases are expected to be stable throughout the lower mantle with (Mg, Fe)SiO_3 post-perovskite and SiO_2 seifertite (α-PbO_2-type, *Pbcn*) stable at core-mantle boundary conditions (~135 GPa). In the case of SiO_2, a further transition to the pyrite-type phase ($Pa\bar{3}$) is observed at 268 GPa (27), but this phase retains 6-fold coordination (sometimes described as 6 + 2). Increases in coordination above six have been reported in SiO_2 glass at ultra-high pressures (28). However, there is no experimental evidence for silicon coordination greater than six in any high-pressure crystalline silicates or their analogues.

While pPv $MgSiO_3$ is the expected silicate phase at the base of Earth's mantle, post-pPv phases with Si-O coordination > 6 may play a decisive role in terrestrial super-Earths of four or

9

greater Earth masses (Suppl. Material, Fig. S1). If the Th_3P_4-type or the closely related partially

disordered $I\bar{4}2d$ phase also exists in Mg_2SiO_4, the change in coordination from 6-fold to 8-fold

may be accompanied by major changes in physical, chemical, and thermodynamic properties.

The ~2.4% volume change associated with the transition is large ($\Delta\rho = $ ~1.5% for Pv to pPv) for

ultra-high pressure phase transitions and may affect the dynamic behavior of the deep mantle.

The Th_3P_4-type phase is related to the proposed tetragonal $I\bar{4}2d$ structure by an order-

disorder transition across cation sites. The expected high internal temperatures of super-Earth

mantles (Suppl. Material, Fig. S1) will likely favor the Th_3P_4-type phase or mostly disordered

$I\bar{4}2d$ structure ($Q = 0.25$) over the completely ordered $I\bar{4}2d$ structure ($Q = 1$). Its intrinsically

disordered nature may also be an important feature as it suggests enhanced miscibility of

chemical components at ultrahigh P-T conditions. Among chalcogenides, Th_3P_4-type phases are

noted for their flexible structure and prevalence of defects, impurities, and disorder (29). This

structural flexibility can affect rheology and transport properties. Compared to other structures,

enhanced phonon scattering in this disordered phase may yield an anomalously low thermal

conductivity (30).

Based on the calculated 0-K transition pressure from pPv to the ordered $I\bar{4}2d$ phase (4),

it is expected that a transition from six-fold coordinated silicate phases to eight-fold coordinated

phases would occur in terrestrial exoplanets greater than about four Earth masses in size. Thus,

the interior dynamics of planets above and below this size range may show important differences

due to the structural phase transition.

In summary, Mg_2GeO_4 adopts the thorium phosphide structure or a highly disordered (Q

= 0.25) tetragonal $I\bar{4}2d$ phase at pressures above ~190 GPa. The phase is calculated to be ~

2.4% denser than the mixture of $MgGeO_3$ post-perovskite and MgO. This is the first

experimental synthesis of a phase with Ge in eight-fold coordination with oxygen and the first occurrence of the Th_3P_4-type phase in an oxide. Just as the discovery of widespread six-coordinated germanates/silicates profoundly altered our understanding of silicate crystal chemistry and its role in the Earth's deep interior, the discovery of an eight-fold coordinated, intrinsically disordered germanate opens the possibility of previously unexplored crystal-chemical behavior in the silicate minerals of large rocky exoplanets. Our results also raise the possibility that this structure or the related $I\bar{4}2d$ structure could also be adopted by other oxide minerals at extreme pressures. Thus, our results suggest the possibility of novel crystal chemistry in A_3O_4- and AB_2O_4-type compounds that warrant further exploration.

Acknowledgments

Experimental methodology

Mg$_2$GeO$_4$ olivine samples were synthesized according to established procedures (21, 31) and confirmed by X-ray diffraction. The sample was mixed with 10 wt.% gold which acted as a pressure calibrant and laser absorber. Rhenium gaskets were pre-indented and ~20 μm diameter holes were laser drilled to form the sample chamber in a diamond anvil cell. The sample + Au pellets were then loaded into a cell with beveled 50-μm culet anvils. No pressure medium was used in order to maximize the X-ray diffraction signal from the sample.

Angle-dispersive X-ray diffraction was carried out at 13-ID-D and 16-ID-B of the Advanced Photon Source using monochromatic X-rays (λ = 0.3344 Å and 0.4066 Å, respectively) focused to dimensions of 3 x 3 μm^2 and 5 x 3 μm^2, respectively. CdTe 1M Pilatus detectors were used to collect the diffraction patterns. LaB$_6$ and CeO$_2$ standards were used to calibrate the detector position and orientation.

High temperatures were attained by double-sided heating with diode pumped fiber lasers with ~10-15 μm spot sizes. Temperature was increased in a stepwise fashion with ~150-200 K steps with a heating duration of 1.5-2 minutes at each step (total heating duration: 7-27 minutes). The laser power was adjusted independently on both sides to keep temperature differences to < 150 K. Temperatures were measured using spectroradiometry. Pressure was determined using the (111) reflection of Au (32). Thermal pressures were accounted for using the Mie-Grüneisen equation of state.

The two-dimensional X-ray diffraction images were integrated to one-dimensional patterns using DIOPTAS (33) and fit using background-subtracted Voigt line shapes. Lattice parameters were calculated by least-squares refinement of the peak positions (34) or whole profile Le Bail refinement as implemented in MAUD (35). For the whole pattern refinement, the

background was fit with a 4th order polynomial, instrumental profile terms were fit with Gaussian Cagliotti terms and sample broadening incorporated isotropic size and strain broadening.

Computational Details

We performed first-principles density functional theory calculations to determine the structural parameters of the $I\bar{4}2d$ and Th_3P_4-type Mg_2GeO_4 phases, constrain the equation of state over the range from 135 - 342 GPa and study the details of the order-disorder transition between the two phases. We simulated the disordered system using the special quasirandom structure method (36, 37) as implemented in the ATAT-toolkit (14). We generated a 224-atom supercell and used the Monte Carlo method to find the most random structure considering clusters up to 6 neighbors as a distance of up to 3.2 Å for a cubic lattice. We constrained the supercell to be doubled in each direction of the cubic cell, i.e. 10.984 Å × 10.984 Å × 10.984 Å for our starting system. QUANTUM ESPRESSO (15) plane wave pseudopotential code PWSCF was used to perform DFT computations, with PBE exchange-correlation, and PAW potentials from the pslibrary pseudopotential library (38) with a 4x4x4 Monkhorst-Pack k-point mesh in the supercell and an energy cutoff for the wavefunctions of 100 Ryd.

References

1.   T. V. Hoolst, L. Noack, A. Rivoldini, Exoplanet interiors and habitability. *Adv. Phys: X.* **4**, 1630316 (2019).

2.   K. Umemoto, R. M. Wentzcovitch, Two-stage dissociation in $MgSiO_3$ post-perovskite. *Earth Planet. Sci. Lett.* **311**, 225–229 (2011).

3.   T. S. Duffy, N. Madhusudhan, K. K. M. Lee, "Mineralogy of super-Earth planets" in *Treatise on Geophysics (2nd Ed.)*, 2nd Ed., G. Schubert, Ed. (Elsevier, 2015), pp. 149–178.

4.   K. Umemoto, S. Wu, M. Ji, C.-Z. Wang, and K.-M. Ho, Phase transitions in $MgSiO_3$ post-perovskite in super-Earth mantles. *Earth Planet. Sci. Lett.* **478**, 40–45 (2017).

5.   M. H. Shahnas, R. N. Pysklywec, D. A. Yuen, Penetrative convection in super-Earth planets: consequences of $MgSiO_3$ postperovskite dissociation transition and implications for super-earth GJ876d. *J. Geophys. Res: Planets.* **123**, 2162–2177 (2018).

6.   A. E. Ringwood, M. Seabrook, High-pressure phase transformations in germanate pyroxenes and related compounds. *J. Geophys. Res.* **68**, 4601–4609 (1963).

7.   C. V. Stan, R. Dutta, R. J. Cava, V. B. Prakapenka, T. S. Duffy, High-pressure study of perovskites and postperovskites in the (Mg, Fe)GeO$_3$ system. *Inorg. Chem.* **56**, 8026–8035 (2017).

8.   K. Hirose, K. Kawamura, Y. Ohishi, S. Tateno, N. Sata, Stability and equation of state of MgGeO$_3$ post-perovskite phase. *Am. Min.* **90**, 262–265 (2005).

9.   K. Umemoto, R. M. Wentzcovitch, Ab initio exploration of post-PPV transitions in low-pressure analogs of MgSiO$_3$. *Phys. Rev. Mater.* **3**, 123601 (2019).

10.   T. Nagai, K. Yano, M. Dejima, T. Yamanaka, Pressure-induced amorphization of Mg$_2$GeO$_4$-olivine. *Miner. J. Japan* **17**, 151–157 (1994).

11.   X. Zhang, V. Stevanović, M. d'Avezac, S. Lany, A. Zunger, Prediction of A$_2$BX$_4$ metal-chalcogenide compounds via first-principles thermodynamics. *Phys. Rev. B* **86**, 014109 (2012).

12.   T. Holland, R. Powell, Thermodynamics of order-disorder in minerals; I, Symmetric formalism applied to minerals of fixed composition. *Am. Min.* **81**, 1413–1424 (1996).

13.   K. Umemoto, R. M. Wentzcovitch, Ab initio prediction of an order-disorder transition in Mg$_2$GeO$_4$: Implication for the nature of super-Earth's mantles. *arXiv:2012.08056 [cond-mat]* (2020).

14.   A. van de Walle, P. Tiwary, M. de Jong, D. L. Olmsted, M. Asta, A. Dick, D. Shin, Y. Wang, L.-Q. Chen, and Z.-K. Liu, Efficient stochastic generation of special quasirandom structures. *Calphad* **42**, 13–18 (2013).

15.   P. Giannozzi, *et al.*, QUANTUM ESPRESSO: a modular and open-source software project for quantum simulations of materials. *J. Phys: Condens. Matter* **21**, 395502 (2009).

16.   H. T. Stokes, D. M. Hatch, FINDSYM: program for identifying the space-group symmetry of a crystal. *J. Appl. Cryst* **38**, 237–238 (2005).

17.   A. Kubo, *et al.*, Stability and equation of state of the post-perovskite phase in MgGeO$_3$ to 2 Mbar. *Geophys. Res. Lett.* **33**, L12S12 (2006).

18.   Y. Kono, *et al.*, Ultrahigh-pressure polyamorphism in GeO$_2$ glass with coordination number >6. *Proc. Natl. Acad. Sci. USA* **113**, 3436–3441 (2016).

19.   T. Kubo, T. Kato, Y. Higo, K. Funakoshi, Curious kinetic behavior in silica polymorphs solves seifertite puzzle in shocked meteorite. *Sci. Adv.* **1**, e1500075 (2015).

20.   C. E. Runge, A. Kubo, B. Kiefer, Y. Meng, V. B. Prakapenka, G. Shen, R. J. Cava, and T. S. Duffy, Equation of state of MgGeO$_3$ perovskite to 65 GPa: comparison with the post-perovskite phase. *Phys. Chem. Miner.* **33**, 699–709 (2006).

21.   R. B. Von Dreele, A. Navrotsky, A. L. Bowman, Refinement of the crystal structure of Mg$_2$GeO$_4$ spinel. *Acta. Cryst. B* **33**, 2287–2288 (1977).

22.   M. Blanchard, K. Wright, J. D. Gale, Atomistic simulation of Mg$_2$SiO$_4$ and Mg$_2$GeO$_4$ spinels: a new model. *Phys. Chem. Miner* **32**, 332–338 (2005).

23.   P. E. Petit, F. Guyot, G. Fiquet, J. P. Itié, High-pressure behaviour of germanate olivines studied by X-ray diffraction and X-ray absorption spectroscopy. *Phys. Chem. Miner.* **23**, 173–185 (1996).

24.   S. Speziale, C.-S. Zha, T. S. Duffy, R. J. Hemley, H. Mao, Quasi-hydrostatic compression of magnesium oxide to 52 GPa: Implications for the pressure-volume-temperature equation of state. *J. Geophys. Res: Solid Earth*. **106**, 515–528 (2001).

25.   S. D. Jacobsen, C. M. Holl, K. A. Adams, R. A. Fischer, E. S. Martin, C. R. Bina, J.-F. Lin, V. B. Prakapenka, A. Kubo, and P. Dera, Compression of single-crystal magnesium oxide to 118 GPa and a ruby pressure gauge for helium pressure media. *Am. Min*. **93**, 1823–1828 (2008).

26.   T. Irifune, A. Ringwood, Phase transformations in subducted oceanic-crust and buoyancy relationships at depths of 600-800 km in the mantle. *Earth Planet. Sci. Lett*. **117**, 101–110 (1993).

27.   Y. Kuwayama, K. Hirose, N. Sata, Y. Ohishi, The pyrite-type high-pressure form of silica. *Science* **309**, 923–925 (2005).

28.   C. Prescher, V. B. Prakapenka, J. Stefanski, S. Jahn, L. B. Skinner, and Y. Wang, Beyond sixfold coordinated Si in SiO_2 glass at ultrahigh pressures. *Proc. Natl. Acad. Sci. USA*. **114**, 10041–10046 (2017).

29.   C. E. Whiting, E. S. Vasquez, C. D. Barklay, Uranium based materials as potential thermoelectric couples for future radioisotope power systems in *2018 IEEE Aerospace Conference*, (2018), pp. 1–9.

30.   G. J. Snyder, E. S. Toberer, "Complex thermoelectric materials" in *Materials for Sustainable Energy*, (Co-Published with Macmillan Publishers Ltd, UK, 2010), pp. 101–110.

31.   P. C. Burnley, The effect of nonhydrostatic stress on the olivine-spinel transformation in Mg_2GeO_4 PhD Thesis, University of California-Davis (1990).

32.   Y. Fei, A. Ricolleau, M. Frank, K. Mibe, G. Shen, and V. Prakapenka, Toward an internally consistent pressure scale. *Proc. Natl. Acad. Sci. USA*. **104**, 9182–9186 (2007).

33.   C. Prescher, V. B. Prakapenka, DIOPTAS: a program for reduction of two-dimensional X-ray diffraction data and data exploration. *High. Press. Res*. **35**, 223–230 (2015).

34.   T. J. B. Holland, S. A. T. Redfern, Unit cell refinement from powder diffraction data; the use of regression diagnostics. *Mineral. Mag*. **61**, 65–77 (1997).

35.   L. Lutterotti, Total pattern fitting for the combined size–strain–stress–texture determination in thin film diffraction. *Nucl. Instrum. Methods Phys. Res. B*. **268**, 334–340 (2010).

36.   S.-H. Wei, L. G. Ferreira, J. E. Bernard, and A. Zunger, Electronic properties of random alloys: Special quasirandom structures. *Phys. Rev. B* **42**, 9622–9649 (1990).

37.   A. Zunger, S.-H. Wei, L. G. Ferreira, and J. E. Bernard, Special quasirandom structures. *Phys. Rev. Lett.* **65**, 353–356 (1990).

38.   A. Dal Corso, Pseudopotentials periodic table: From H to Pu. *Comp. Mater. Sci* **95**, 337–350 (2014).

Fig. 1 X-ray diffraction patterns of the Th$_3$P$_4$-type phase of Mg$_2$GeO$_4$ at 161 GPa, 225 GPa, and 275 GPa. The two lower pressure patterns are collected upon quench to 300 K after heating to 1806 K and 3650 K respectively, whereas the upper pattern was collected *in situ* at 2020 K. Peaks from Th$_3$P$_4$-type Mg$_2$GeO$_4$ are indicated with Miller indices.
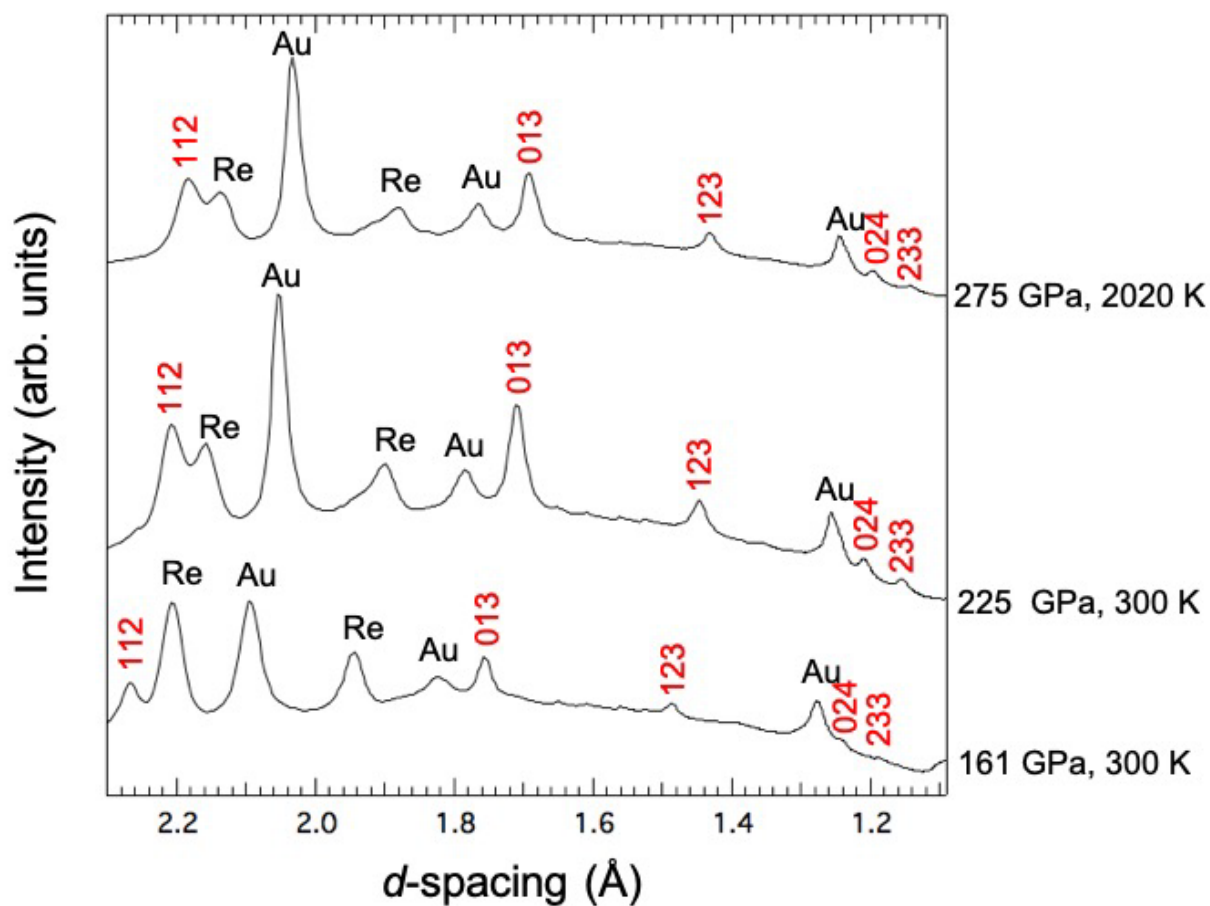
Fig. 2(a) Order-disorder transition between $I\bar{4}2d$ and $I\bar{4}3d$ Mg$_2$GeO$_4$ from DFT calculations (solid black line). The red circles indicate the isostructural transition from mostly ordered (Q = 0.8125) to mostly disordered (Q = 0.25) $I\bar{4}2d$ structure. The dashed line shows the transition curve from Ref. 16. **(b)** Variation in c/a with order parameter at 200 GPa; triplets, quadruplets and sextuplets are the different SQS cluster sizes. **(c)** Comparison of the observed X-ray diffraction pattern (black) at 187 GPa, 2010 K with the theoretically calculated structures with Q = 0.8125 (blue), Q = 0.25 (green) and Q = 0 (red) at 200 GPa. The FWHM of the observed sample peaks has be used as Gaussian broadening for the simulated patterns.

2
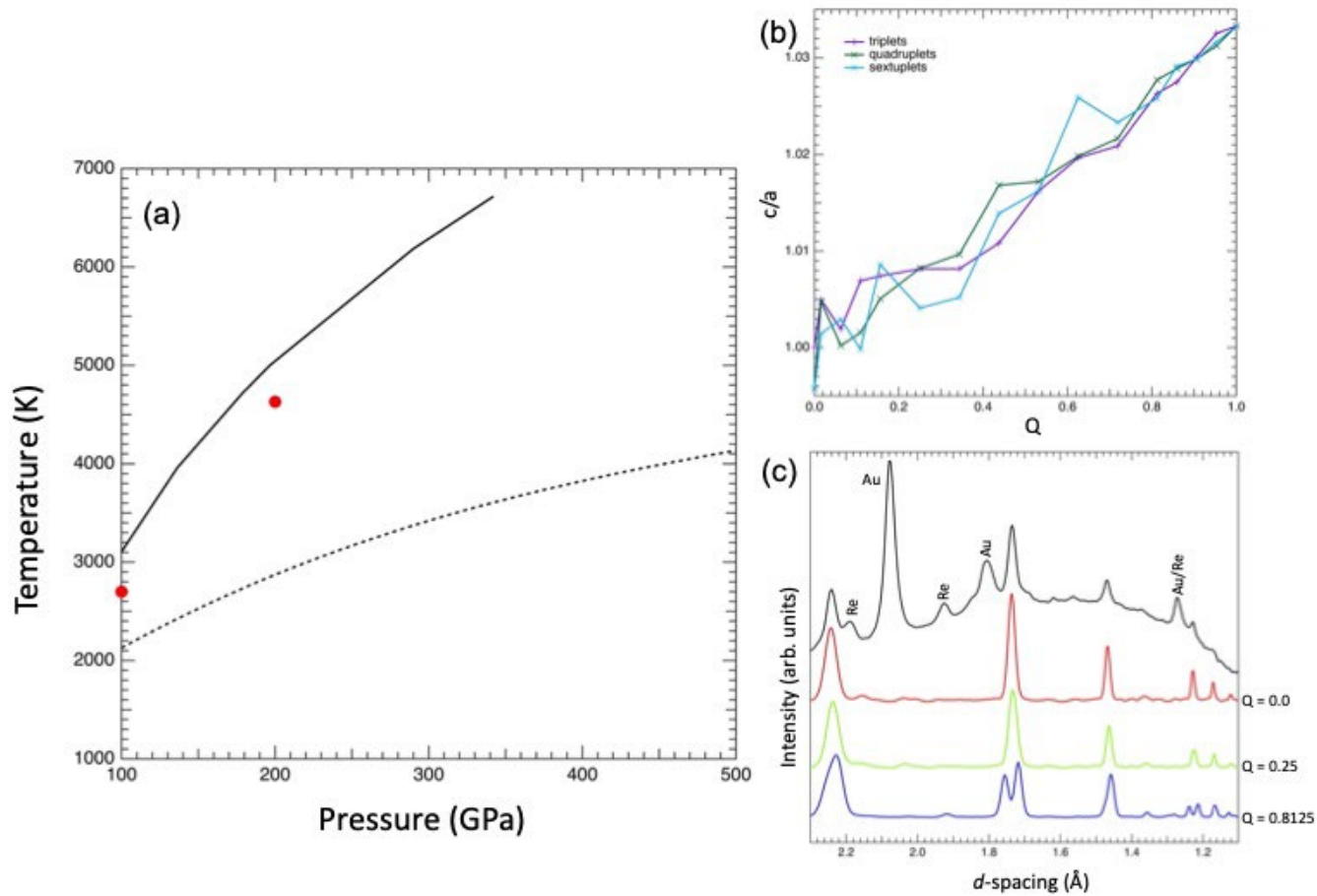
Fig. 3(a) Rietveld refinement of the X-ray diffraction pattern (black) obtained after heating Mg_2GeO_4 to 3650 K at 240 GPa with subsequent quenching to room temperature ($a = 5.4055$ (2) Å, $O_x = 0.0468$). Red and green curves show the fit and background, respectively. Miller indices of the Th_3P_4-type Mg_2GeO_4 are shown above the observed diffraction pattern. A small amount of untransformed starting material is present near 1.95 A. **(b)** Structure of the Th_3P_4-type phase: Red spheres are oxygen atoms and orange/mauve spheres represent the Mg/Ge site with shading to indicate 2/3 occupancy by Mg and 1/3 occupancy by Ge. A representative $(Mg,Ge)O_8$ polyhedron is also shown.
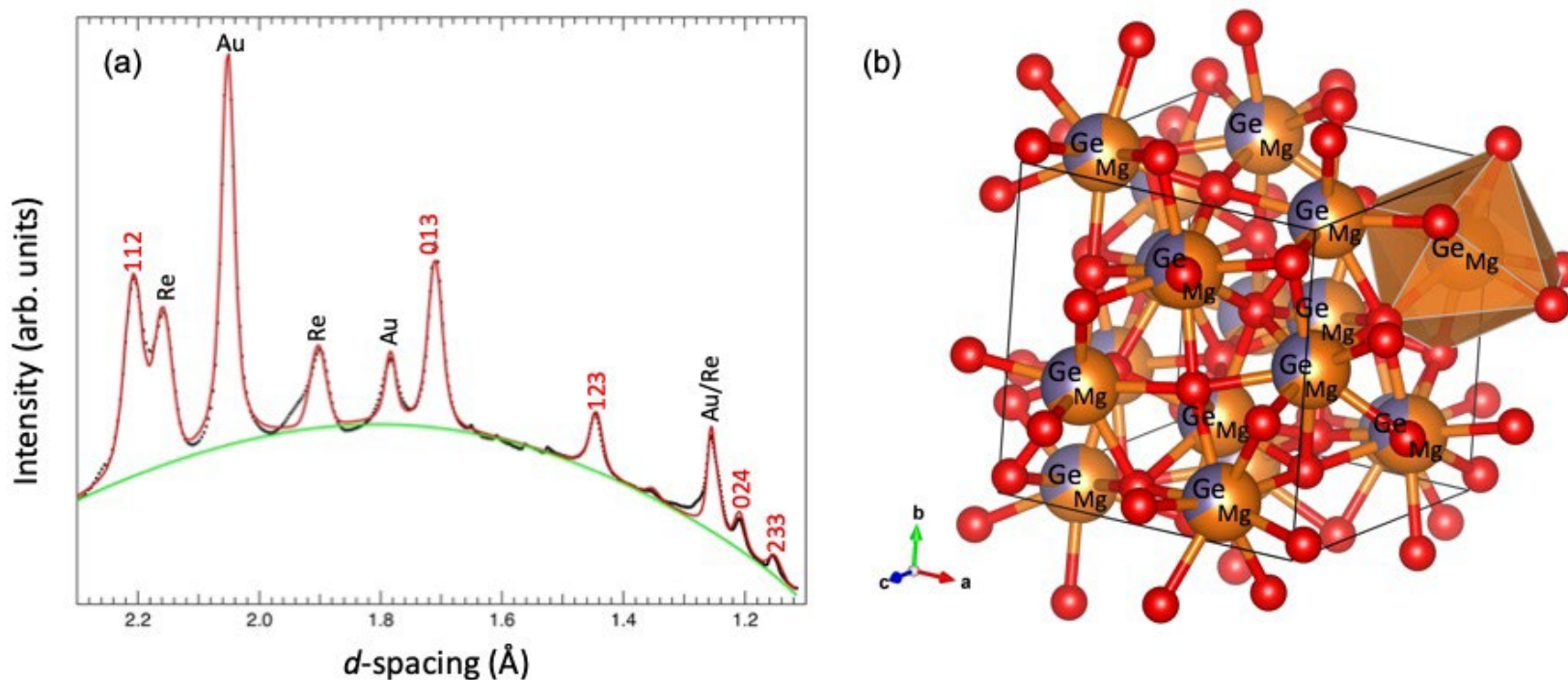
Fig. 4(a) Phase diagram of Mg_2GeO_4. Solid brown circles indicate P-T conditions where only $MgGeO_3$ pPv + MgO is observed. The solid red circles show P-T conditions where diffraction patterns showed only Th_3P_4-type Mg_2GeO_4 phase. The open red circles show lower temperature conditions at which Th_3P_4 phase is observed, but is interpreted as metastable. The solid grey symbols indicate conditions at which diffraction from both pPv and Th_3P_4 are observed, but the pPv peaks grow and the Th_3P_4 peaks diminish with increasing heating time and/or temperature (panel b). The growth of pPv at the expense of Th_3P_4 is taken as evidence that pPv is the stable phase at these conditions. Conversely, the solid pink symbols show conditions at which the peaks of the Th_3P_4 phase are observed to grow and the pPv peaks diminish with heating time and/or temperature (panel c). This is evidence that the Th_3P_4 phase is stable at these conditions. The black line is the estimated phase boundary for the pPv + MgO→ $I\bar{4}3d$ Mg_2GeO_4 from this work. Open brown diamonds are P-T points at which pPv was observed in previous work (17). The stability regions for pPv+MgO, pPv + MgO with metastable Th_3P_4 at lower temperatures, and Th_3P_4 are indicated at the bottom. **(b)** Diffraction patterns during a heating cycle at 169 GPa showing the growth of post perovskite peaks (brown circles) at the expense of Th_3P_4 peaks (red circles). **(c)** Diffraction patterns during a heating cycle at 175 GPa showing the growth of Th_3P_4-type phase (indicated by red circles) and decreased intensity of the pPv phase (indicated by brown circles).
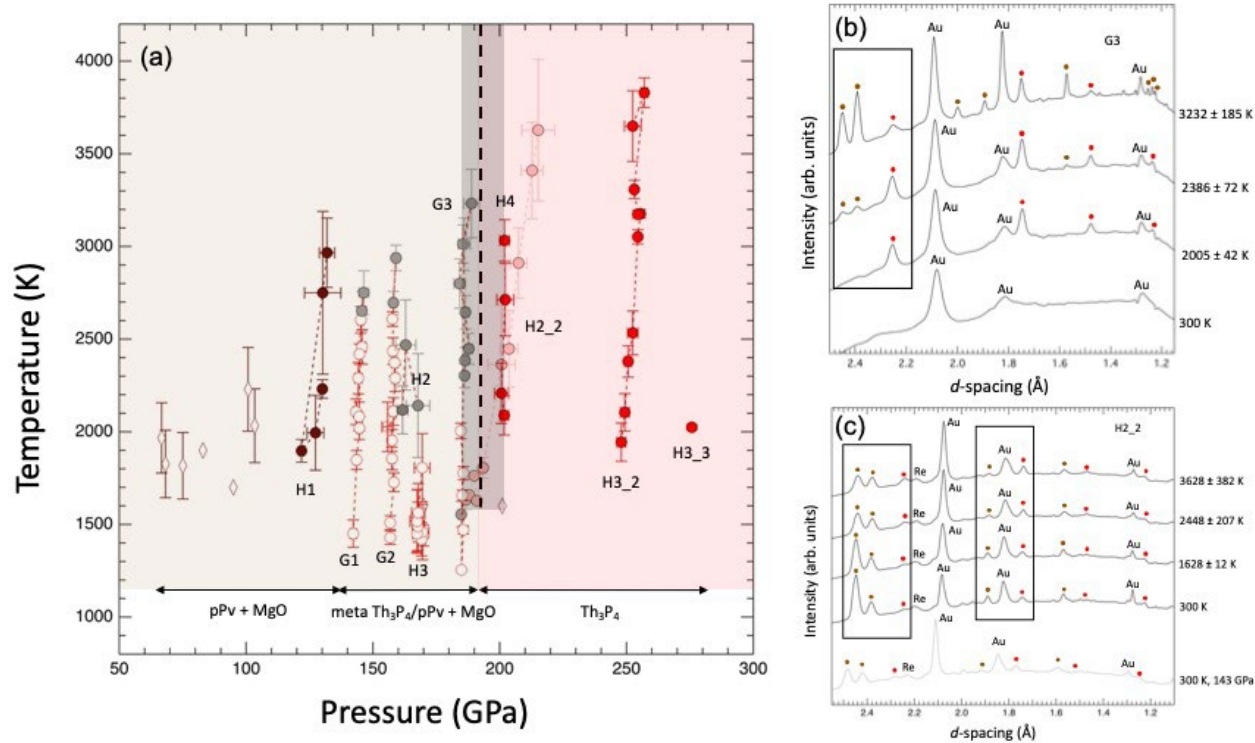
Fig. 5(a) Equation of state of the Th_3P_4-type phase from experiments (300 K, solid red circles) and theoretical calculations (0 K, open red circles). Lines are 3rd order Birch-Murnaghan equation fits. **(b)** Densities of selected phases in the MgO-GeO$_2$ system. Solid circles are from this work (brown: pPv; red: Th_3P_4). Previous studies are indicated by open symbols, brown diamonds: pPv (16); green triangles: Pv (20); purple square: spinel (21, 22); black stars: olivine (23); blue hexagons: B1-MgO (24, 25). The brown and green solid lines are the calculated densities of mixtures of MgGeO$_3$ Pv and pPv with MgO.